Effects of Different Stratospheric SO$_2$ Injection Altitudes on Stratospheric Chemistry and Dynamics

Simone Tilmes[1,2] , Jadwiga H. Richter[2], Michael J. Mills[1] , Ben Kravitz[3] ,
Douglas G. MacMartin[4,5] , Rolando R. Garcia[1] , Douglas E. Kinnison[1] ,
Jean-Francois Lamarque[2] , Joseph Tribbia[2] , and Francis Vitt[1]

[1] Atmospheric Chemistry, Observations, and Modeling Laboratory, National Center for Atmospheric Research, Boulder, CO, USA, [2] Climate and Global Dynamics Laboratory, National Center for Atmospheric Research, Boulder, CO, USA, [3] Atmospheric Sciences and Global Change Division, Pacific Northwest National Laboratory, Richland, WA, USA, [4] Mechanical and Aerospace Engineering, Cornell University, Ithaca, NY, USA, [5] Department of Computing and Mathematical Sciences, California Institute of Technology, Pasadena, CA, USA

Key Points:
- Very similar surface cooling can be achieved with stratospheric SO$_2$ injections at 1 and 5 km above the tropopause (at 15°N and 15°S)
- The 33% more injection is required for the low-altitude injection case, resulting in significantly stronger heating of the tropical stratosphere
- Chemical and dynamical changes explain differences in the column ozone response to SO$_2$ injections between high- and low-altitude injections

Abstract Strategically applied geoengineering is proposed to reduce some of the known side effects of stratospheric aerosol modifications. Specific climate goals could be reached depending on design choices of stratospheric sulfur injections by latitude, altitude, and magnitude. Here we explore in detail the stratospheric chemical and dynamical responses to injections at different altitudes using a fully coupled Earth System Model. Two different scenarios are explored that produce approximately the same global cooling of 2°C over the period 2042–2049, a high-altitude injection case using 24 Tg SO$_2$/year at 30 hPa (≈25-km altitude) and a low-altitude injection case using 32 Tg SO$_2$/year injections at 70 hPa (between 19- and 20-km altitude), with annual injections divided equally between 15°N and 15°S. Both cases result in a warming of the lower tropical stratosphere up to 10 and 15°C for the high- and low-altitude injection case and in substantial increases of stratospheric water vapor of up to 2 and 4 ppm, respectively, compared to no geoengineering conditions. Polar column ozone in the Northern Hemisphere is reduced by up to 18% in March for the high-altitude injection case and up to 8% for the low-altitude injection case. However, for winter middle and high northern latitudes, low-altitude injections result in greater column ozone values than without geoengineering. These changes are mostly driven by dynamics and advection. Antarctic column ozone in 2042–2049 does not recover from present-day (2002–2009) values for both cases.

1. Introduction

Geoengineering using sulfur injections into the stratosphere has been proposed as a method to deliberately counteract global warming as a result of anthropogenic climate change (Crutzen, 2006). However, enhanced stratospheric aerosol burden also impacts the balance between photochemical production, loss, and large-scale transport of stratospheric ozone and therefore impacts column ozone. Earlier studies showed that geoengineering may significantly delay the recovery of the Antarctic ozone hole (Heckendorn et al., 2009; Pitari et al., 2014; Tilmes et al., 2008, 2009).

Increased stratospheric ozone depletion has been observed after the large tropical volcanic eruption of Mt. Pinatubo in 1991, which led to a strongly enhanced stratospheric sulfate aerosol layer (e.g., Portmann et al., 1996). Ozone depletion was also observed after smaller middle- and high-latitude eruptions, for example, of the Sarychev volcano in 2009 (Berthet et al., 2017) and Calbuco in 2015 (Ivy et al., 2017). Besides significant changes of 3–5% in global ozone observed after large volcanic eruptions in recent decades (World Meteorological Organization, 2010), column ozone also has been subject to significant changes in the last 40 years as a result of increasing of ozone-depleting substances (ODSs) in the stratosphere. Maximum abundance of ODSs was reached around 2000 (Newman et al., 2006). Largest impacts of ODS were observed in the recurring ozone hole in southern spring over Antarctica, which already shows signs of recovery in recent years (Solomon et al., 2016). Additionally, ozone is impacted by changes in greenhouse gases (World Meteorological Organization, 2014). In particular, the removal of ODS and the projected acceleration of the Brewer-Dobson Circulation (BDC) in a future climate is expected to lead to a superrecovery and, therefore, an increase the ozone column (e.g., Hegglin & Shepherd, 2007). Following the Representative Concentration Pathway RCP8.5,

a significant increase in column ozone well above its historical level is projected, especially in middle to high latitudes and, with that, a reduction in surface ultraviolet (UV) radiation (Butler et al., 2016).

The changes in column ozone as the result of stratospheric aerosol geoengineering in a future climate will therefore strongly depend on greenhouse gas abundance as well as the evolution of ODSs in the stratosphere. Net changes in column ozone also depend on the magnitude of the injections (Heckendorn et al., 2009) and, therefore, on the timing of the application and on the specifics of the aerosol distribution (Pitari et al., 2014; Xia et al., 2017). Various model experiments have been performed to explore how the location of the stratospheric injection of sulfur dioxide (SO_2) and sulfuric acid (H_2SO_4) impacts aerosol distribution and climate (e.g., English et al., 2012; Heckendorn et al., 2009; Kleinschmitt et al., 2017; Niemeier et al., 2011; Niemeier & Schmidt, 2017; Pierce et al., 2010). These studies have shown that injections at higher altitudes in the tropics, about 5 km above the tropopause, are more efficient in reducing global surface temperatures than injections at lower altitudes, unless relatively large injections around 40 Tg SO_2/year or more are considered (Niemeier & Schmidt, 2017). However, none of these studies included interactive stratospheric chemistry, aerosol formation, radiation, and climate.

The focus of this study is to explore changes in stratospheric chemistry and dynamics that result from injecting SO_2 at two different altitudes while reaching similar global surface temperature reduction between 2042 and 2049 under the RCP8.5 scenario (Meinshausen et al., 2011). Instead of using injections at the equator, we use combined injections at 15°N and 15°S, which produces a more spatially uniform aerosol optical depth (AOD) distribution (MacMartin et al., 2017). It was also shown to be more efficient in reducing the top of the atmosphere radiative imbalance and surface temperature if injected at 25 km. Furthermore, in contrast to injections at the equator, injections outside the equator do not increase the period of the quasi-biennial oscillation (QBO; Richter et al., 2017).

For injections at lower stratospheric altitudes, gases and particles were shown to move faster toward middle and high latitudes compared to injections at higher altitudes, which reduces their stratospheric lifetime, reduces their effect on global temperatures, and changes the distribution of the aerosols (Tilmes et al., 2017). Therefore, larger amounts of SO_2 are required for lower-altitude injections to reach the same surface cooling effect as for higher-altitude injections. Understanding differences in the impact of injection altitudes on the stratospheric composition is important for estimating benefits and side effects of different injection strategies.

Model simulations in this study were performed with the Whole Atmosphere Community Climate Model (WACCM) running as the atmospheric component of the Community Earth System Model Version 1, denoted hereafter by CESM1(WACCM). The details of the model setup are described in section 2. We further summarize the specifics of the simulations performed in section 2.1 and give an overview of the resulting climate outcomes in section 2.2. In section 3, we first summarize changes in column ozone as a result of differences in the SO_2 injection altitudes and thereafter discuss important processes that result in differences in stratospheric dynamics and chemistry between low- and high-altitude injections at 15°N and 15°S. Our discussion and conclusions are in section 4.

2. Experimental Setup

We use CESM1(WACCM) as described in detail by Mills et al. (2017). This fully coupled Earth System model runs with a horizontal resolution of 0.95° in latitude by 1.25° in longitude with 70 vertical levels extending from the surface to 145 km. The model includes comprehensive stratospheric chemistry and is interactively coupled to atmospheric dynamics including an internally generated QBO, aerosol microphysics, radiation, and climate (Mills et al., 2017). For the simulations, we couple the Community Atmosphere Model version 5 (CAM5), the Community Land model version 4.0 (CLM4.0), the Parallel Ocean Program version 2 (POP2), and the Los Alamos sea ice model (CICE Version 4). The land model was run with interactive carbon and nitrogen cycles, and the atmospheric and land components are coupled to the chemistry. Simulations were carried out on the Yellowstone high-performance computer platform (Computational and Information Systems Laboratory, 2012).

2.1. Simulations

A control simulation was performed starting in 1975 using WACCM, following historical emissions until 2005 and RCP8.5 (Meinshausen et al., 2011) after the year 2005, with steadily increasing greenhouse gas
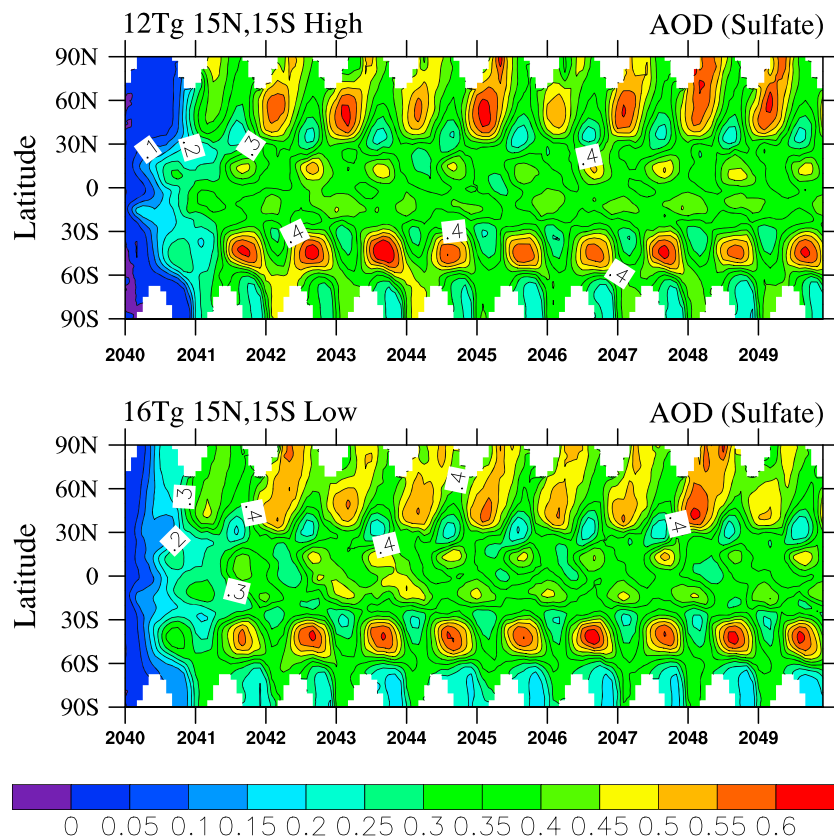
Figure 1. Enhanced aerosol optical depth (AOD) in the visible (550 nm) as the result of stratospheric sulfur injections compared to the control between 2040 and 2049 for simultaneous single-point injections at 15°N and 15°S of 12 TgSO_2/year at each location (total of 24 TgSO_2/year at about 25 km (30 hPa) altitude (top panel) and 16 TgSO_2/year per injection location (total 32 TgSO_2/year) at about 20-km (70 hPa) altitude (bottom panel).

concentrations through the year 2100, as described in Morgenstern et al. (2017). In addition, we performed a WACCM simulation for the period 1955–1975 to represent preozone hole conditions.

For the geoengineering simulations, two 10-year simulations starting from year 2040 of the control simulation were performed, where SO_2 was continuously injected at two single-point locations at one longitude (180°E) and at two different altitude levels: a low-altitude injection case at ≈1 km above the tropopause and a high-altitude injection case at 5 km above the tropopause. The injection amount for each of these cases was determined from earlier simulations, as described by MacMartin et al. (2017), who showed that the low-altitude injection case requires an injection rate that is 33% higher than in the high-altitude injection case. Total annual injection amount of 24 Tg of SO_2 per year, where 12 Tg SO_2/year is injected at each latitude location (15°N and 15°S and at 30 hPa altitude), resulted in a global surface cooling of about 2°C between 2042 and 2049.

The low-altitude injection simulation required a total annual injection amount of 32 Tg of SO_2 per year, where 16 Tg SO_2/year are injected at each latitude location (15°N and 15°S and at 70-hPa altitude), to reach a similar amount of cooling. The aerosol burdens increase for about 2 years before reaching a steady state distribution (see also Tilmes et al. (2017) and MacMartin et al. (2017)). Column total stratospheric sulfate optical depth shows a very similar pattern for the two different cases, with little interannual variation in the tropics, and larger variations in middle and high latitudes (Figure 1). In the following, averages for the period between 2042 and 2049 are considered, to exclude the first 2 years before the aerosol burden has reached steady state. Larger adjustments in particular in the surface temperature are expected in the first 3–4 years in both injection cases (e.g., Tilmes et al., 2017).
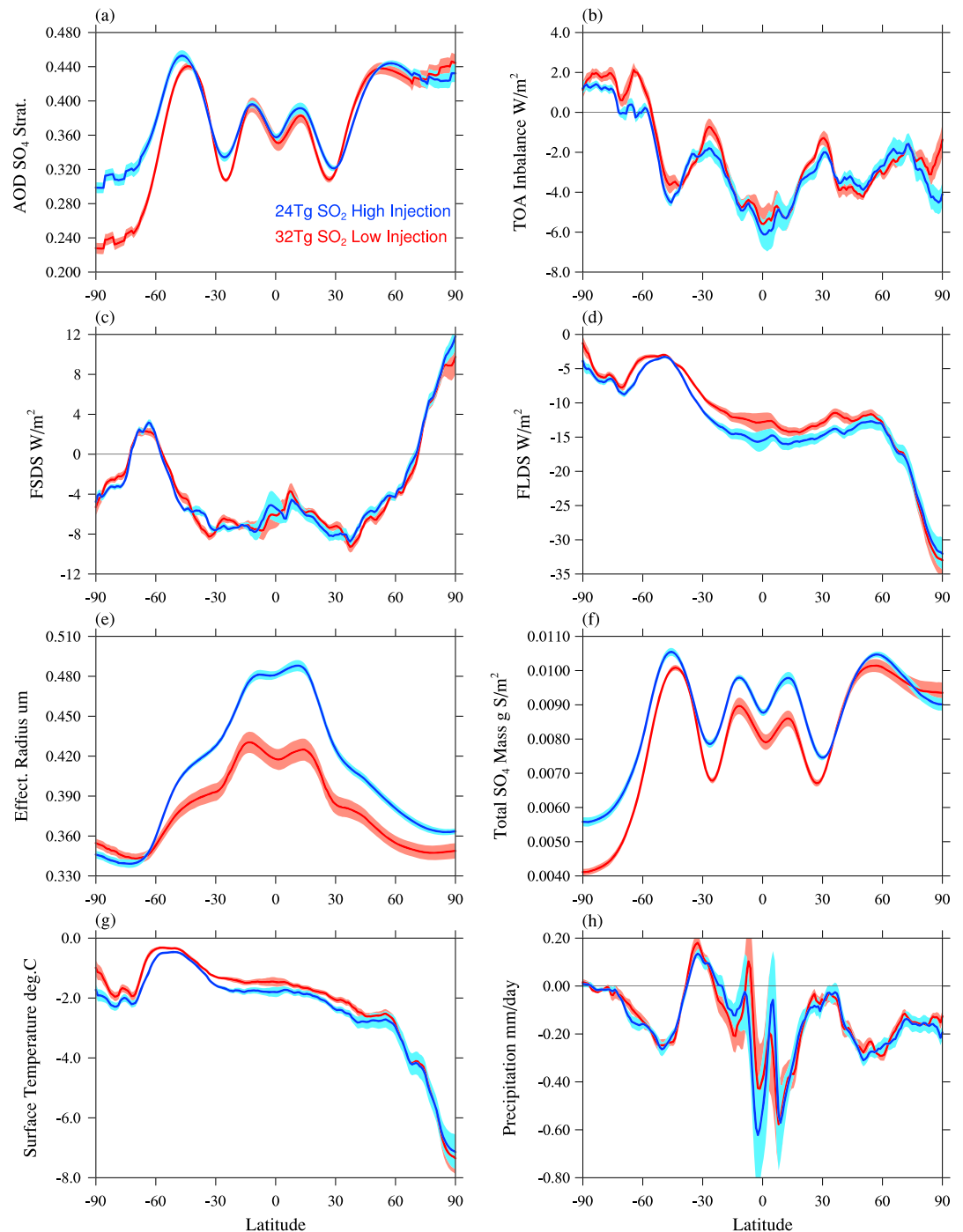
Figure 2. Differences between sulfur injection cases at high altitude (blue) and low altitude (red) and the control of zonally and annually averaged variables averaged for 2042 and 2049, for aerosol optical depth in the visible (550 nm) as the result of stratospheric sulfur injections (a), top of the atmosphere (TOA) radiative imbalance (b), radiative forcing of shortwave downwelling radiation at the surface (FSDS; c), radiative forcing of longwave downwelling radiation at the surface (FLDS; d), effective radius (e), sulfate mass burden (f), surface temperature (g), and precipitation (h). Shaded regions indicate 1 standard deviation of annual means.
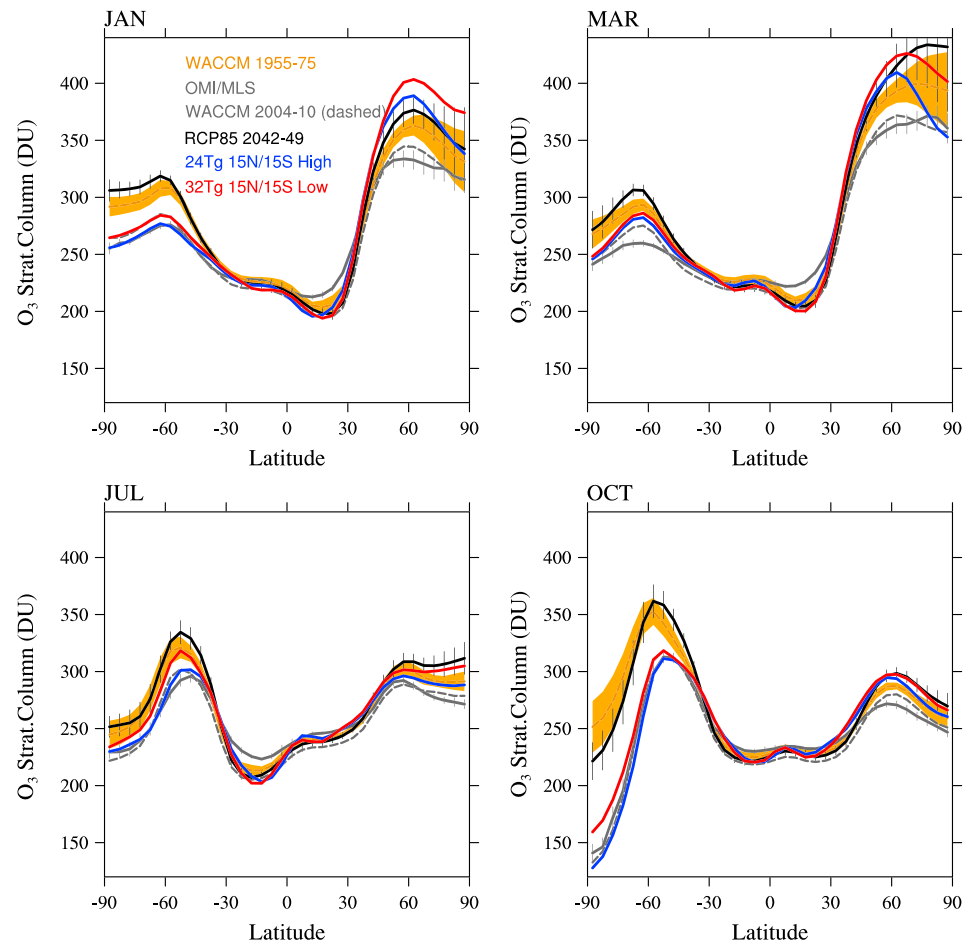
Figure 3. Monthly and zonally averaged stratospheric ozone column (in DU) comparison between Ozone Monitoring Instrument/Microwave Limb Sounder (OMI/MLS) observations between 2004 and 2010 (gray), and Whole Atmosphere Community Climate Model (WACCM) simulations (for ozone >150 ppb in the model): control simulation between 2004 and 2010 (gray dashed lines) and between 2042 and 2049 (black), for the high-altitude injection experiment (blue) and for the low-altitude experiment (red), for January, March, July, and October (different panels). Error bars for the observations in gray describe the zonally averaged 2-sigma 6-year root mean square standard error of the mean at a given grid point, derived from the gridded product (Ziemke et al., 2011). Model results are interpolated to the same grid and error bars (only shown for the control simulations) indicate the standard deviation of the interannual variability per latitude interval. WACCM results between 1955 and 1975 that indicate preozone hole conditions are shown in orange including standard deviation (shading).

2.2. Resulting Climate Response

The two simulations reach very similar zonal mean AOD, resulting in very similar radiative forcing and surface temperature changes for both injection cases (see Figure 2). There are, however, still some differences in the resulting aerosol size distribution and location. AOD changes following the SO_2 injections of the high- and low-altitude injection cases are very similar for the tropics and Northern Hemisphere (NH) middle and high latitudes (Figure 2a). For the low-altitude injection case, slightly smaller AOD values occur around 30° in latitude in both hemispheres, and in particular in the Southern Hemisphere (SH) high latitudes. Low-altitude injections result in a shallower stratospheric aerosol distribution and faster removal of aerosols through the low branch of the BDC (Tilmes et al., 2017). This likely results in less aerosol entering the SH polar vortex, which is a strong transport barrier during austral winter and spring (Figure 2a). Despite these differences, both simulations show similar reductions in the top of the atmosphere radiative imbalance (Figure 2b) and the shortwave (SW) downwelling radiation at the surface (FSDS; Figure 2c). Top of the atmosphere imbalance in high latitudes is similar for both cases, despite larger differences in AOD, especially in the SH. This is in particular the case in winter and spring, when AOD changes are lowest in high SH polar latitudes with lack of sunlight. Despite larger injection rates for the low-altitude injection case, the total SO_4 mass burden
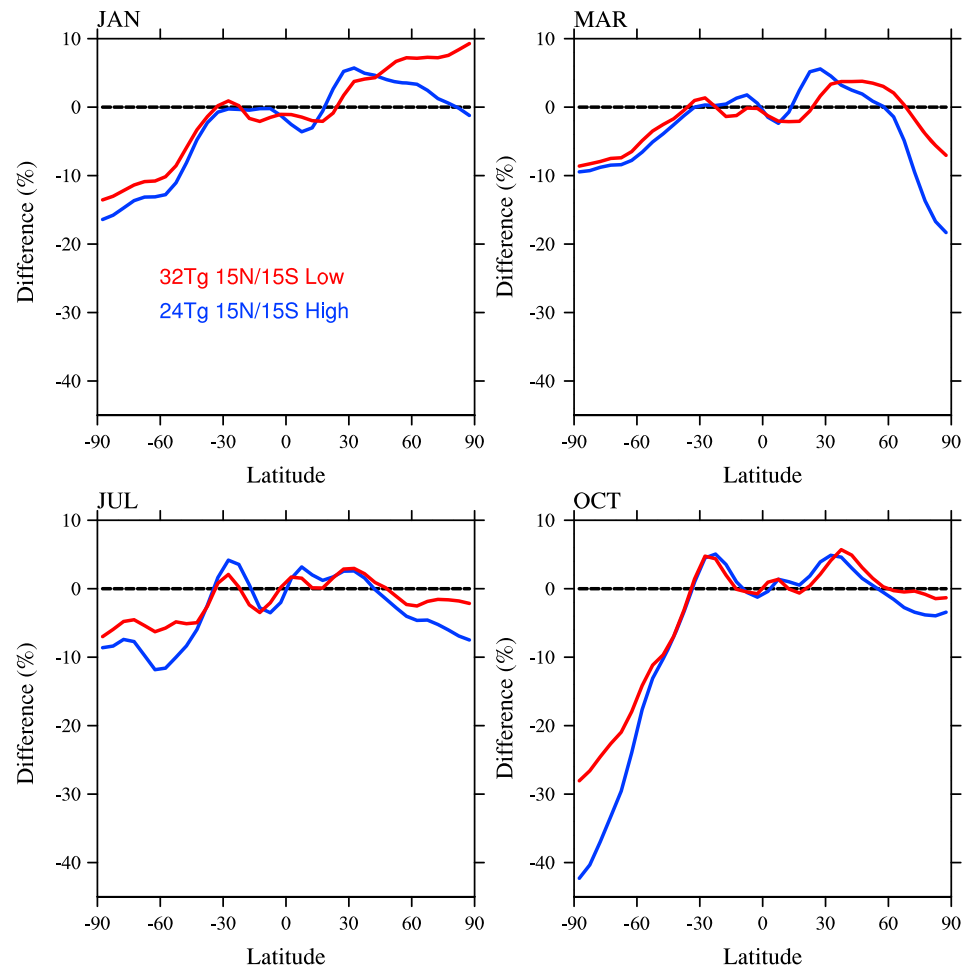
Figure 4. Differences of monthly and zonally averaged stratospheric ozone column (in %) between the two sulfur injection experiments and the control simulation averaged between 2042 and 2049, as shown in Figure 3.

in the stratosphere is smaller (Figure 2f), due to a faster removal of particles (Tilmes et al., 2017). On the other hand, the size of aerosol particles, and therefore the effective radius, is smaller (Figure 2e), as discussed in section 3.2, producing a greater radiative effect per unit mass and compensating for the faster removal.

The downwelling longwave (LW) radiation at the surface (FLDS) is strongly reduced compared to the control simulation. Reductions in FSDS as the result of the aerosol layer reflecting UV radiation reduce latent and sensible heat fluxes at the surface (not shown) and reverse the increase in LW radiation from the atmosphere to the surface as the result of increasing greenhouse gases. FLDS is more strongly reduced (by about 2% or 3 W/m^2) in the high-altitude injection case than in the low-altitude injection case for low and middle latitudes (Figure 2d). Since FLDS is affected by radiative fluxes from the atmosphere above the surface, these changes are likely caused by adjustments in the atmospheric heating induced by absorption of radiative flux by the aerosols, changes in greenhouse gases (especially water vapor), and changes in clouds. As we will discuss in section 3, water vapor in the stratosphere is significantly increased in the low-altitude injection case, causing a positive forcing that counteracts the reduction in SW radiation due to SO$_2$ injections. Consistent with changes in FLDS, surface temperatures show a slightly stronger reduction in the high-altitude injection case as compared to the low-altitude injection case, with exceptions in high northern latitudes. On average both simulations reduce surface temperature by about 2°C. Small differences in surface temperature between the two cases could be further adjusted by slightly increasing the injection amount of the low-altitude injection case; however, they are not expected to change the stratospheric response significantly. Differences in precipitation changes are not significant in the zonal mean (Figure 2h), and regional differences are also mostly not significant (not shown).
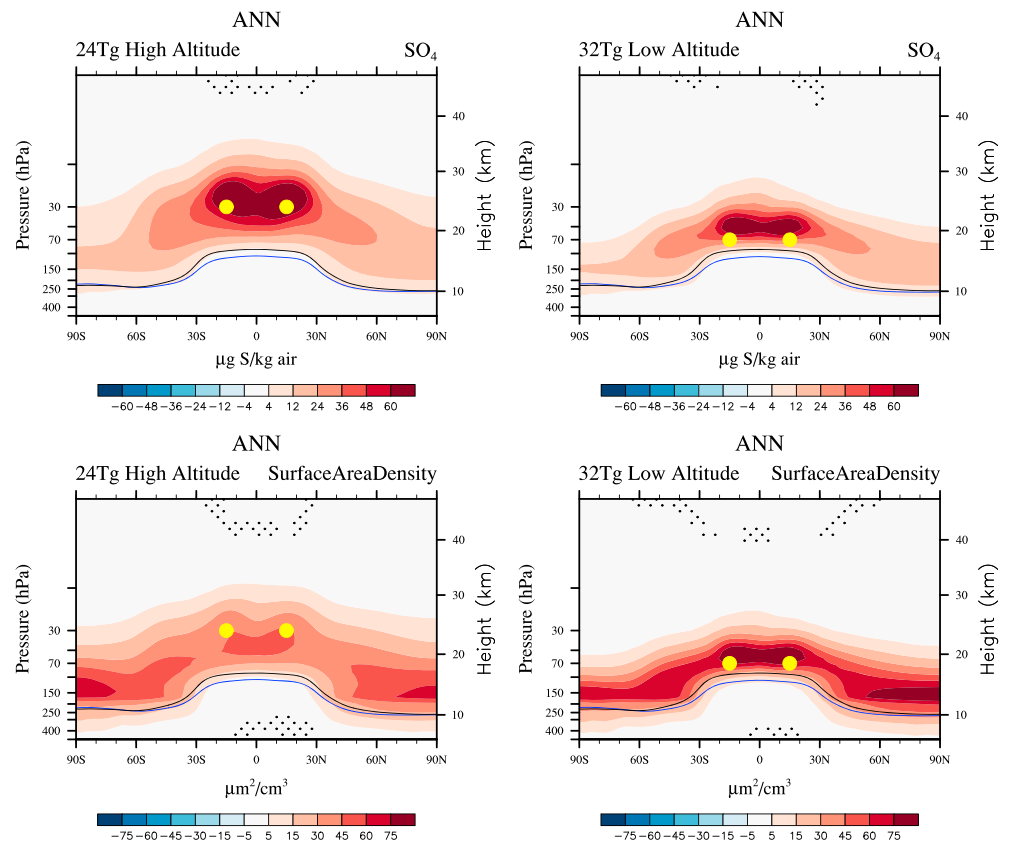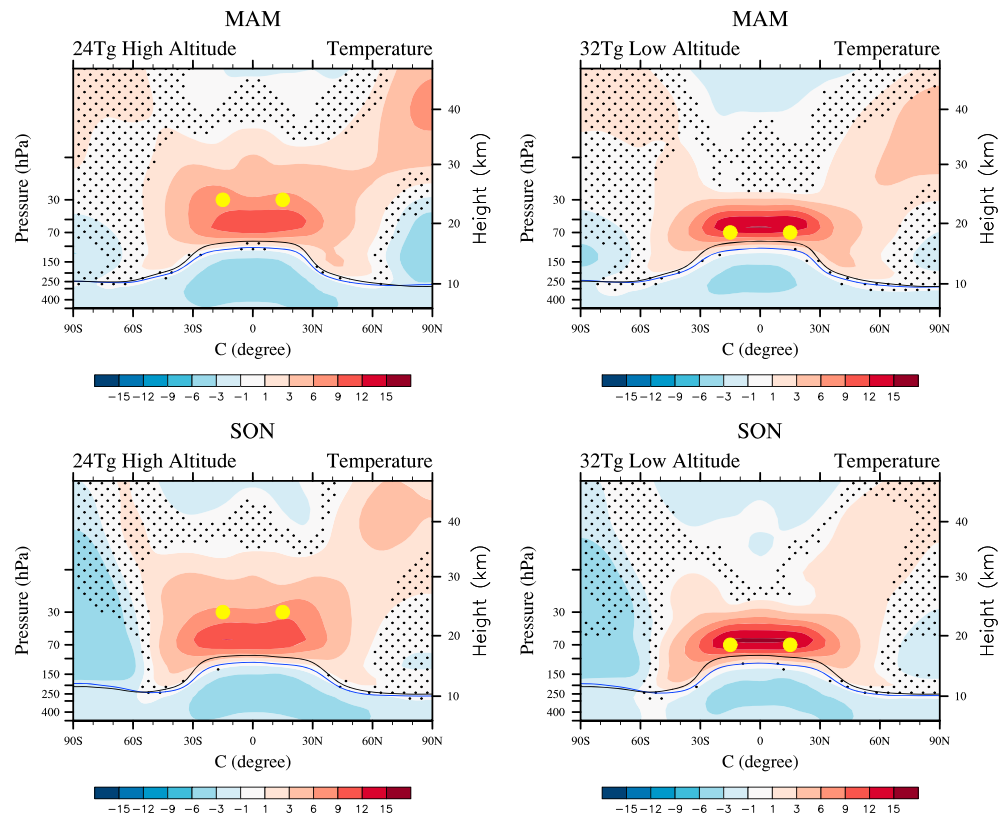
Figure 5. Differences between the two sulfur injection cases at high altitude (left) and low altitude (right) and the control of zonally and annually averaged variables between years 2042 and 2049, for SO_4 (first row) and surface area density (second row). The lapse rate tropopause is indicated as a black line for the control and a blue line for the SO_2 injection cases. Areas of nonsignificant difference at the 95th percentile level to the control are marked as small black dots. Yellow dots are locations of injection.

3. Changes in Stratospheric Composition and Dynamics

In contrast to the similar surface temperature effects in our experiments (which were obtained by design), injections at different altitudes result in large differences in the stratospheric composition, including aerosol mass, spatial distribution, and aerosol effective radius, as well as the chemical composition. Those differences are driven by changes in stratospheric temperatures and interactions with dynamics including water vapor and transport, as well as changes in chemical ozone loss cycles. Injections of SO_2 at different altitudes consequently impact column ozone differently. In this section, we first describe change in column ozone as the result of SO_2 injections at different altitudes in comparison to preozone hole and present-day conditions (aligned with available observations between 2004 and 2010) and then discuss reasons for the differences between the two simulations as the result of changes in the stratospheric composition and dynamics.

3.1. Column Ozone Change

As explored in this study, the impact of geoengineering on column ozone depends on the aerosol distribution as a result of different injection altitudes (Figure 3). Stratospheric column ozone in the control simulation 2004 and 2010 (Figure 3, gray dashed line) compares very well for different seasons and regions to that observed by Ozone Monitoring Instrument/Microwave Limb Sounder for the same period (gray solid line), as also shown in Mills et al. (2017). The seasonality, including the depth of the ozone hole with minimum values in stratospheric column ozone of around 120-130 DU, is also well represented. The period investigated here, between 2042 and 2049, shows clear signs of ozone recovery with regard to 2004–2010 (black solid line). The largest changes are obvious in Northern and Southern Hemisphere high latitudes in spring. By 2042–2049, the ozone hole over Antarctica mostly disappeared without geoengineering and is similar to preozone hole values based on WACCM results in 1955–1975 (dashed orange line with orange shading). For the NH high and middle latitudes, the largest increase in column ozone occurs during spring (up to 80–100 DU for 60–90°N) as the result

Figure 6. Zonally averaged differences in temperature (in degrees C) between each of the two sulfur injection cases at high altitude (left) and low altitude (right) and the control for the average of years 2042 and 2049 for March/April/May (MAM; first row) and September/October/November (SON; second row). The lapse rate tropopause is indicated as a black line for the control and a blue line for the SO$_2$ injection cases. Areas of nonsignificant difference at the 95th confidence level to the control are marked as small black dots. Yellow dots are locations of injection.

of reduced ODS as well as changes in stratospheric transport and temperature. Only a small increase in stratospheric column ozone of less than 10 DU (less than 5%) is simulated for the tropics, consistent with earlier studies (Butler et al., 2016).

The two SO$_2$ injection experiments between 2042 and 2049 impact column ozone differently depending on location and season. Both experiments result in a decrease in column ozone over middle and high latitudes in the SH for all seasons, offsetting the recovery between 2004–2010 and 2042–2049 (Figures 3 and 4, bottom right). The low-altitude injection case shows somewhat less reduction in column ozone (28%) during the ozone hole season over the South Pole, while the high-altitude injection case shows up to 40% decrease in ozone, which results in similar column ozone compared to model results and observations in 2004–2010 (Figures 3 and 4).

Over the NH high latitudes in spring, the high-altitude injection case results in significantly smaller column ozone values (up to 18% reduction in March) compared to the control simulation in 2042–2049. These values are, however, very close to column ozone in 2004–2010. On the other hand, the low-altitude injection case shows smaller column ozone reductions of 8% in spring compared to the control. Both injection cases produce larger column ozone values than the control simulation between 2042 and 2049, especially between 30°N and 60°N and for October to March. Values reach up to 8% above the control simulation in January for the low injection case, which is well above preozone hole values. No significant differences in column ozone between the different experiments are obvious in the tropics. Processes that contribute to these differences are described in the following sections.

3.2. Aerosols and Surface Area Density
Different injection locations for SO$_2$ affect the formation and transport of sulfate aerosols. The high-altitude injection case shows larger mass and larger effective radii than the low-altitude injection case, with the
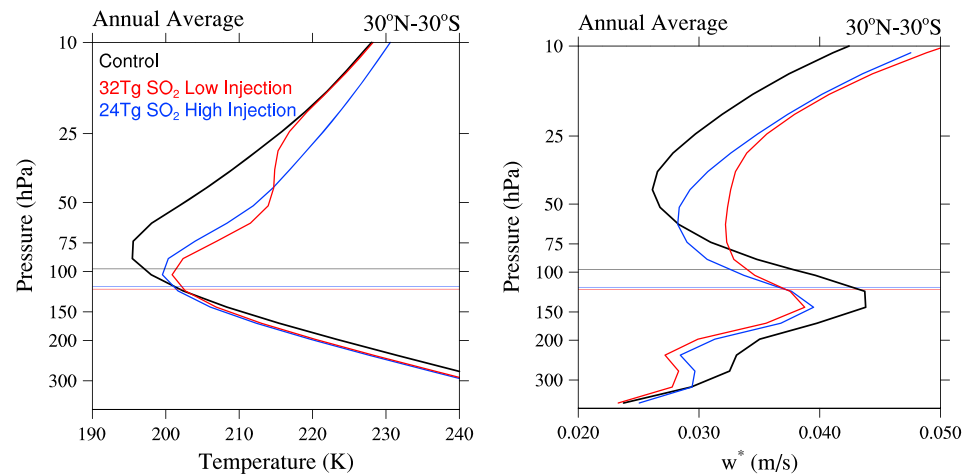
Figure 7. Zonally and annually averaged temperature (left) and residual vertical velocity ($w*$), averaged between 30°N and 30°S for the control simulation (black), and the two injection cases (colored), see legend. The lapse rate tropopause altitude is indicated as black horizontal lines for the control and blue and red horizontal lines for the high and low SO_2 injection cases, respectively.

maximum of both fields in the tropics (Figures 2e and 2f and 5, top row). Differences in mass and effective radius between the two cases result in a very different distributions of aerosol surface area density (SAD; Figure 5, second row). In the high-altitude injection case, SO_2 is transported upward through the deep branch of the BDC, resulting in longer stratospheric residence times and therefore a longer lifetime of aerosols. Increased coagulation with existing particles results in the increase of the effective radius. For the low-altitude injection case, gas and aerosols mostly remain in the shallow branch of the BDC where they are removed faster, and less mass accumulates in the stratosphere (Tilmes et al., 2017).

The region with largest SAD values is located within about 15 and 10 km above the tropopause for the high- and low-altitude injection case, respectively (Figure 5, second row). However, SAD values reach their largest values in the tropics and at high latitudes, where the aerosol mass is smaller and hence the effective radius is small. Furthermore, SAD reaches much larger values for the low-altitude injection case compared to the high-altitude injection case, as the result of the prevalence of smaller aerosols. Larger SAD increases chlorine activation through heterogeneous reactions on liquid aerosol surfaces, resulting in more chemical ozone depletion, as discussed in section 3.5.

3.3. Temperature and Water Vapor

In both injection cases, stratospheric temperatures show significant warming of up to 10 and 15°C for the high- and low-altitude injection cases, respectively (Figure 6). The large heating of the lowermost tropical stratosphere is the result of both radiative and adiabatic heating (Richter et al., 2017). The radiative heating change is the result of increased absorption in mostly the LW as well as in the SW component due to increased aerosol mass, and changes in SW due to changes in ozone. Changes in the sum of LW and SW heating are balanced by adiabatic heating, which is proportional to changes in the residual vertical velocity (Richter et al., 2017). The low injection case shows a more confined area of strongly increased temperatures in the tropics as compared to the high injection case. Seasonally dependent statistically significant temperature changes occur in the lower polar stratosphere in NH winter (not shown) and spring (Figure 6, top row), especially for the high-altitude injection case, consistent with a stronger polar jet stream. Furthermore, significant warming occurs in the upper stratosphere high northern latitudes for both cases.

Temperature increases in the tropical stratosphere and temperature decreases in the troposphere further result in a downward shift of the tropopause (both cold point and lapse rate; (World Meteorological Organization, 1957)), as shown in Figure 7, left panel. Significant increases in tropical temperatures close to the cold point tropopause by about 5 and 7°C for the high and low injection case, respectively, have direct consequences for the amount of water vapor that can enter the stratosphere (e.g., Heckendorn et al., 2009). We see an increase of water vapor of up to 2 ppm for the high injection case and an increase around 4 ppm
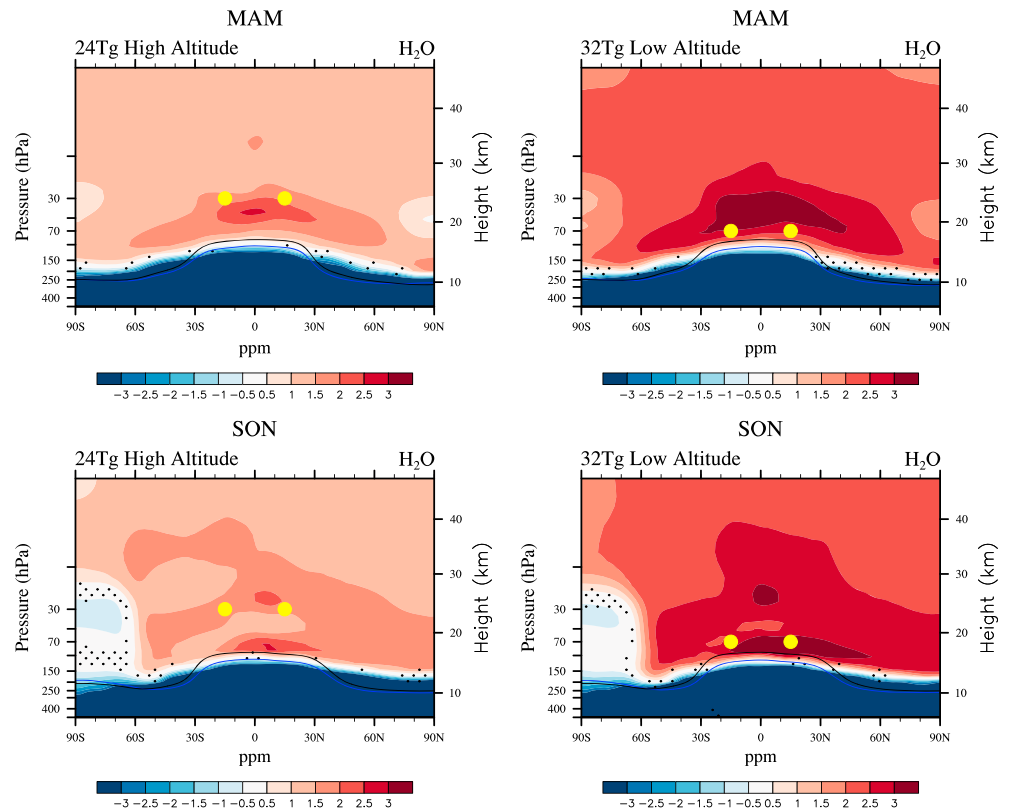
Figure 8. Zonally averaged differences in water vapor mixing ratios between the two sulfur injection cases at high altitude (left) and low altitude (right) and the control for the average of years 2042 and 2049 for March/April/May (MAM; first row) and September/October/November (SON; second row). The lapse rate tropopause is indicated as a black line for the control and a blue line for the SO$_2$ injection cases. Areas of nonsignificant difference at the 95th percentile level are marked as small black dots. Yellow dots are locations of injection.

for the low injection case, as compared to the background value of tropical water vapor being 3–5 ppm. In addition, water vapor is a greenhouse gas, so these changes are expected to result in a strong climate feedback.

Besides the strong increase of water vapor in most of the stratosphere, water vapor significantly decreases in the lower stratosphere over Antarctica during the Austral winter and spring (shown for September/October/November in Figure 8), which corresponds with the temperature reduction and dehydration in the SH polar vortex. NH polar vortex water vapor is not reduced, as the result of warmer temperatures and a weaker polar vortex. In comparison to MLS observations for present day, this model setup has a low bias of approximately 0.5–1 ppm (Mills et al., 2017). Without this bias, the dehydration may be even stronger in the injection simulations.

3.4. Stratospheric Transport and QBO

Geoengineering affects stratospheric transport through two main changes: the surface cooling of the troposphere as the result of reduced incoming SW radiation and the strong increase of tropical temperatures in the stratosphere caused by the enhanced stratospheric sulfate aerosol layer (Figure 7, left panel). Furthermore, the vertical component of the residual circulation ($w^\star$) is reduced below the injection locations while it increases above the injection locations compared to the control conditions (Figure 7, right panel), similar to what was found by Pitari et al. (2014). The decrease in the temperature gradient between the tropics and midlatitudes above the subtropical jet results in a weakening of the subtropical jets for both the high- and low-altitude injection cases (Figure 9, top panel) and in a weakening of the Eliassen-Palm (EP) Flux divergence (which is caused by changes in large-scale planetary waves) atop the subtropical jets (Figure 10, second row). Background values of EP Flux divergence are negative in this region, and positive anomalies translate to a weakening of this quantity. These changes are expected consequences of a weakening of the Hadley cell and a reduction in $w^\star$ below the injection altitude.
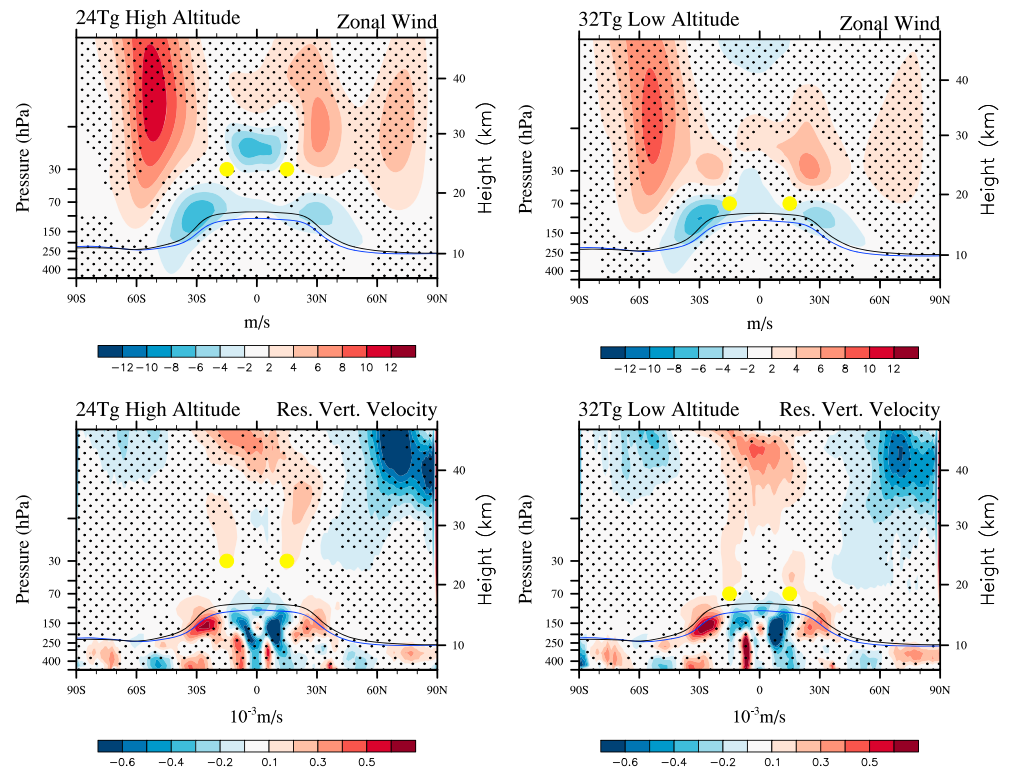
Figure 9. As Figure 5 but for zonal wind (first row), residual vertical velocity $w^\star$ (second row).

The increase in upwelling in the tropics above the injection locations and the increased downwelling in high latitudes in accord with an acceleration of the meridional mean circulation is consistent with the strengthening of the Gravity Wave drag and the EP Flux divergence in middle and high latitudes. In particular, Gravity Wave drag is strongly increased (indicated by negative values) in high polar latitudes for both the high- and low-altitude injection cases (Figure 10, first row). These changes are also aligned with the strengthening of the polar jets in particular in winter and spring for each hemisphere for the high-altitude injection case (Figure 9, top row). Changes in the background temperature structure further influence wave dissipation. There is a stronger increase in the strength of the polar jet for the high compared to the low-altitude injection case, as further discussed below. This difference is likely a result of the greater vertical extent of tropical warming and a stronger increase in the horizontal temperature gradient at higher altitudes in the high-altitude injection case compared to the low-altitude injection case.

The impact of changes in gravity and planetary waves on the BDC can be summarized by looking at changes in the mean mass transport, illustrated by the streamlines of the Transformed Eulerian-mean mass stream function that are based on nongeostrophic eddy transport in the zonal mean flow (Birner & Bönisch, 2011), Figure 10 (bottom row). Changes due to geoengineering, as described above, result in a strengthening of BDC above about 75 hPa and a weakening just above the tropical tropopause. The acceleration of the BDC in the middle stratosphere between 75 and 30 hPa is significantly stronger for the low-altitude injection case than for the high-altitude injection case. A more detailed look at the seasonal changes of the zonal wind and differences between the two cases supports the stronger equatorial westerly wind for the low-altitude injection case (Figure 11). Significant differences are also visible for the polar jet stream in both hemispheres with a significant strengthening of the SH and NH polar jet for all seasons for the high-altitude injection case. This further results in a stronger temperature reduction in high polar latitudes during winter and spring for the high compared to the low-altitude injection case (Figure 6).

The changes in zonal wind and $w^\star$ discussed above interact with the QBO (Figure 12). The mean period of the QBO in this version of CESM1(WACCM) is ≈24 months in present day (Mills et al., 2017). Due to the changing climate the QBO is already altered in the control simulation between 2040 to 2049 relative to present day, with lengthened westerly and shortened easterly phases (Richter et al., 2017). Figure 8b of Richter et al. (2017)
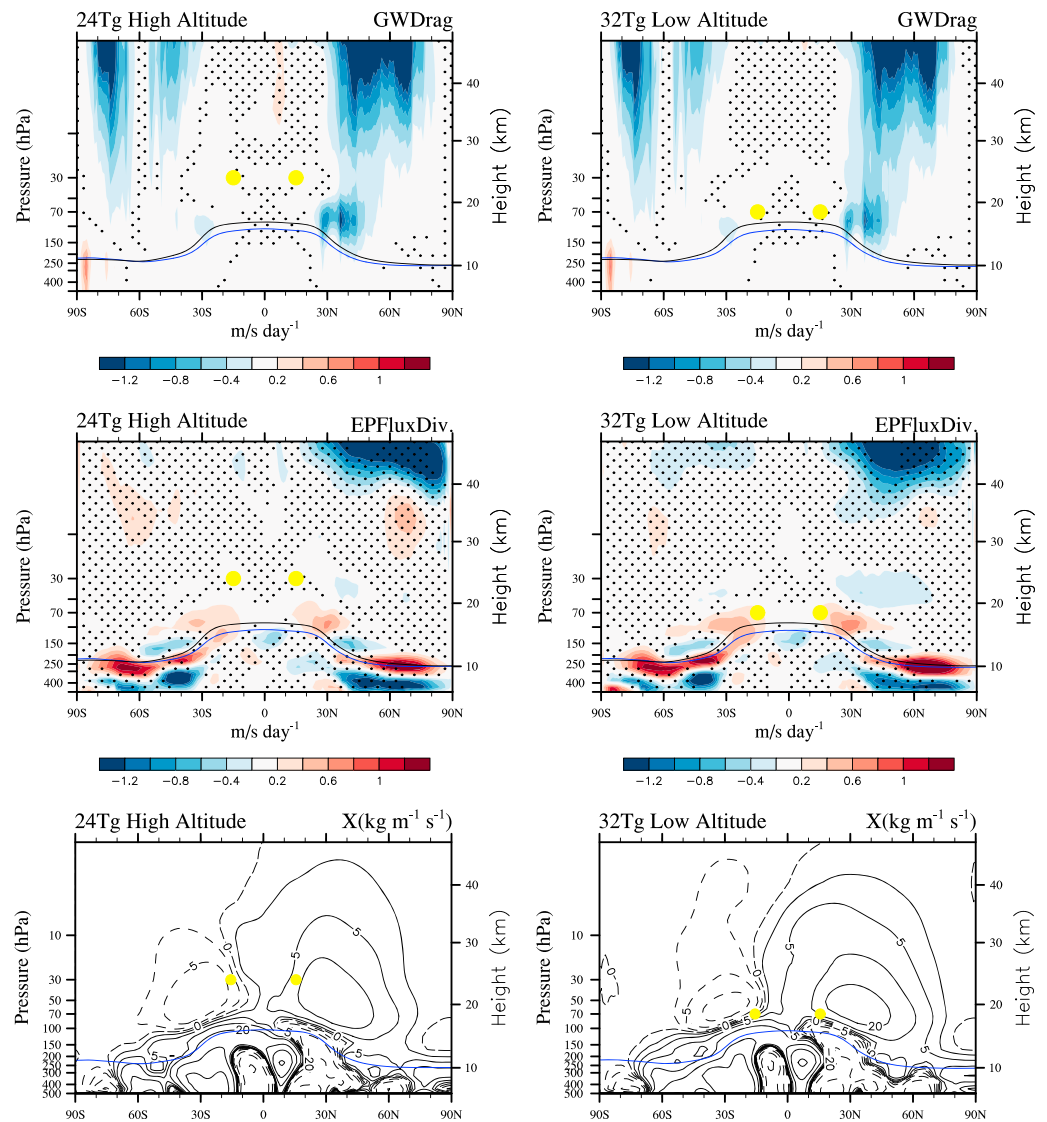
Figure 10. As Figure 5 but for gravity wave drag (first row), Eliassen-Palm flux divergence (second row), and annually averaged Transformed Eulerian-mean stream functions, X (third row). The lapse rate tropopause is indicated as a black line for the control (not shown in the third row) and a blue line for the SO_2 injection cases.

is repeated here in the top panel of Figure 12. In the high-altitude injection case, the mean winds in the tropics weaken between 20 and 30 hPa, while for the low-altitude injection case, they strengthen (Figure 9, top, left panel). For the low injection case easterly winds below 50 hPa become more easterly (Figure 9, top, right panel). In the tropics, the $w\star$ increase is stronger for the low-altitude injection case (Figure 9, bottom row) and these changes result in a lengthening of the westerly phase of the QBO compared to the control, while the easterly phase is stronger below 50 hPa (Figure 12). For the low-altitude injection case, the easterly phase of the QBO is elongated and the westerly phase is shortened, similar to the control case between 2040 and 2049. In contrast, the QBO in the high injection case is quite regular, and closer to present-day conditions. These findings are based on a relatively short period of simulations that do not allow for a complete evaluation of QBO periods and characteristics, and as discussed in Mills et al. (2017) and Richter et al. (2017). The present model is deficient in the representation of the QBO below 70 hPa due to low vertical resolution.

### 3.5. Change in Long-Lived Stratospheric Tracers

The response of stratospheric chemical tracers to geoengineering using sulfur injection is complicated, since tracers are impacted by both changes in dynamics and chemistry. Long-lived tracers, for example, nitrous oxide (N_2O), chlorofluorocarbons (CFCs), inorganic nitrogen oxides (NO_y), and inorganic chlorine oxides
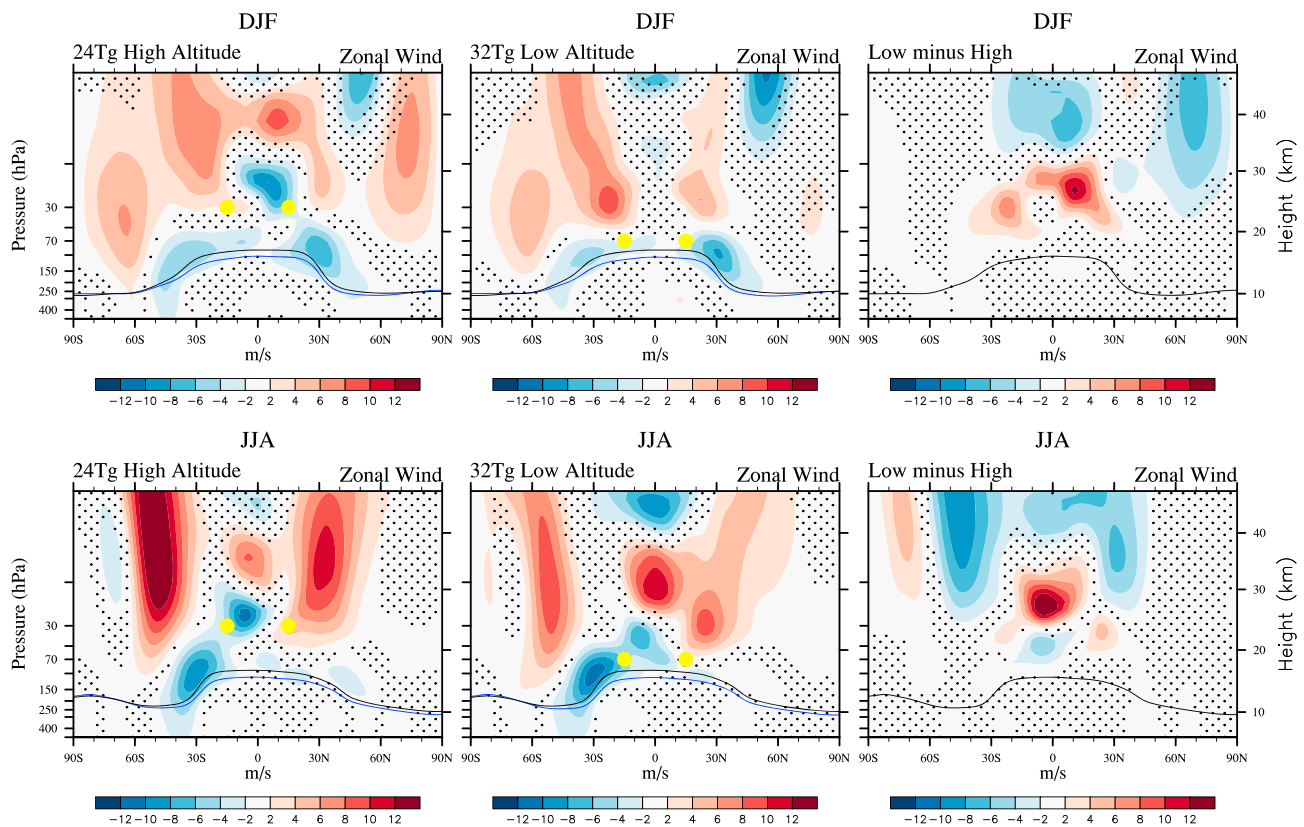
Figure 11. Zonal wind differences between each of the two sulfur injection cases at high altitude (left) and low altitude (middle) and the control for the average of years 2042 and 2049, for December, January, and February (DJF), top row, and for June, July, and August (JJA), bottom row. Differences between the low-altitude injection case and the high-altitude injection case are shown on the right. Areas of nonsignificant difference at the 95th percentile level to the control are marked as small black dots. The lapse rate tropopause is indicated as a black line for the control and a blue line for the SO$_2$ injection cases. Yellow dots are locations of injection.

(ClO$_y$), and bromine oxides (BrO$_y$), are primarily impacted by changes in advection. Figure 13 shows differences of these tracers between the geoengineering and the control simulation for both, high-altitude injection (left) and low-altitude injection (middle). Differences between the two cases are shown on the right. Tracers with mixing ratios that decrease with altitude in the stratosphere show a reduction in mixing ratios below about 23 km, and an increase above (top rows). The reduced vertical advection in the low tropical stratosphere slows the tracer transport in this region. On the other hand, stronger vertical advection in the tropics above about 20 km in the geoengineering case as compared to the control increases vertical transport and causes stronger advection toward higher latitudes, thereby changing the concentration gradient of these tracers. A stronger $w^\star$ for the low-altitude injection case results in a stronger increase of these tracers above 23 km in the tropics. Furthermore, a significant decrease in mixing ratios of these tracers in the lowermost stratosphere and polar regions below about 25 km can be the result of both stronger downwelling of tracers in high latitudes and stronger horizontal transport from the tropics to high latitudes. In contrast to N$_2$O and CFC12, the climatological mixing ratios of NO$_y$ and ClO$_y$ increase with altitude in the stratosphere, with NO$_y$ showing a maximum around 40 km, more similar to ozone. Changes in advection as described above lead to an increase in NO$_y$, ClO$_y$ (and BrO$_y$, not shown) in the lowermost stratosphere, and a decrease above. An additional increase of NO$_y$ occurs above 40 km. Some changes in tracer abundance, in particular in the tropics and the middle-latitude lower stratosphere, may be also caused by changes in photolysis rates, as the result of changes in ozone. On the other, potential changes in UV due to the increase in stratospheric aerosol burden are not included in this model but would have an additional impact (Pitari et al., 2014; Visioni, Pitari, Aquila, Tilmes, et al., 2017). The impact of geoengineering on the stratospheric lifetime of these tracers and exchange between the lowermost stratosphere and troposphere should be investigated in future studies.

Differences between the low- and high-altitude injection cases are consistent with these changes in advection. The low-altitude injection case shows a stronger tropical upwelling above 30 hPa, indicated by larger
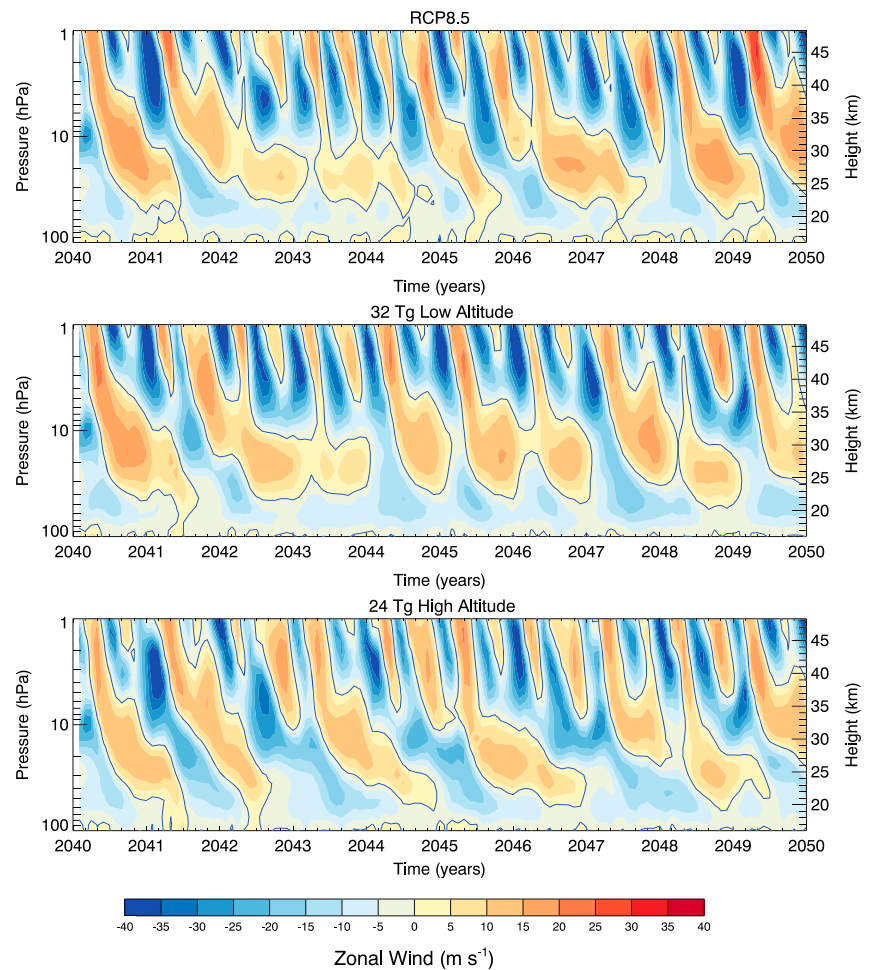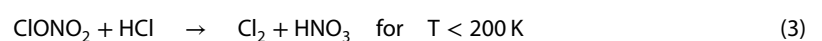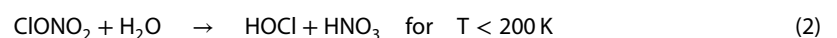
Figure 12. Zonal mean zonal wind, averaged between 2°S and 2°N for years 2040–2049 for the control simulation (top), low-altitude injection case (middle), and high-altitude injection case (bottom). The zero value is indicated by black lines.
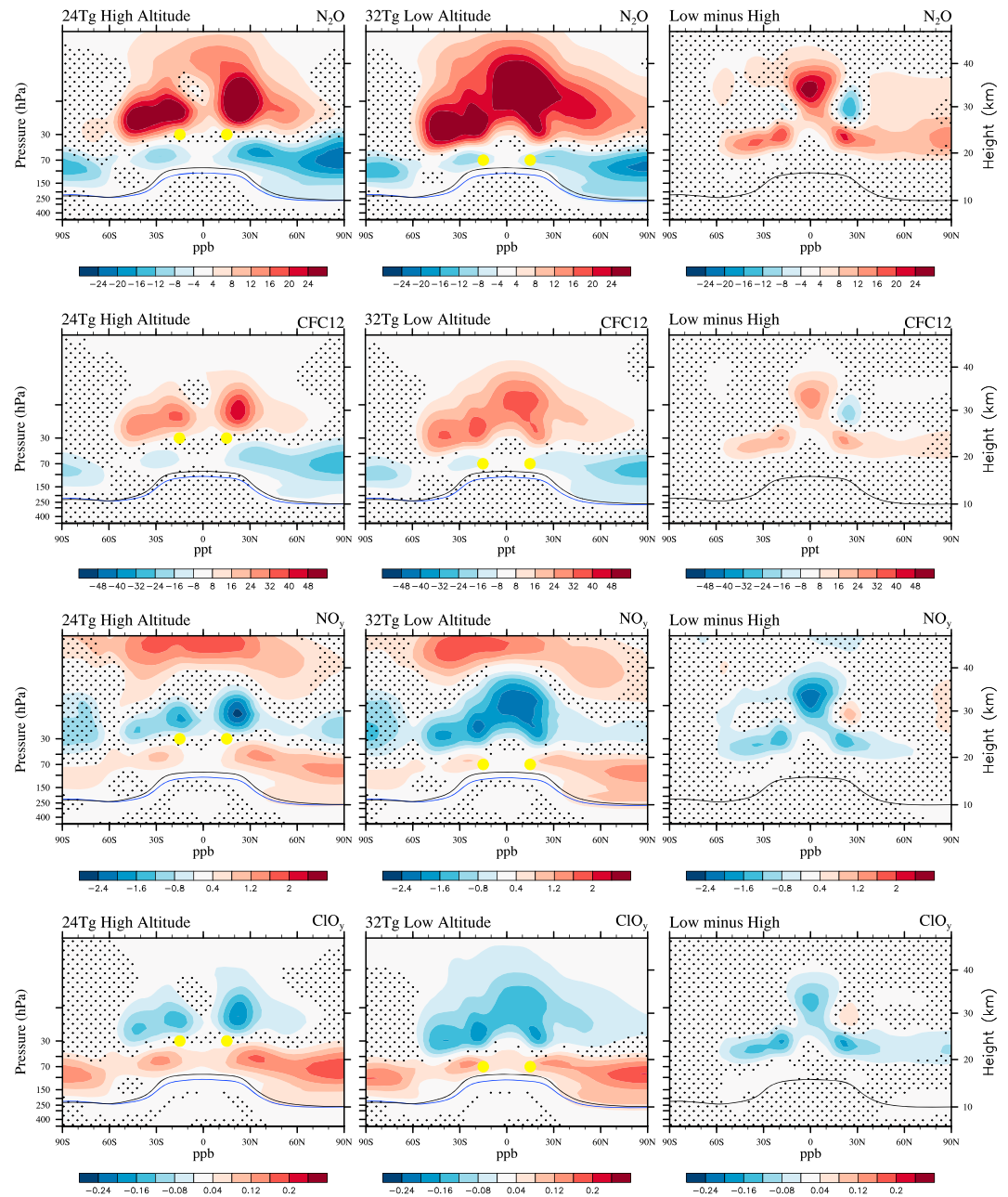
mixing ratios of N_2O and CFC12, and lower mixing ratios of NO_y and ClO_y in the tropical stratosphere above the injection location, and stronger horizontal tracer transport between 30 and 70 hPa, as compared to the high-altitude injection case. Changes in these long-lived tracers impact the abundance of reactive tracers including inorganic nitrogen, chlorine, and bromine which impact ozone loss rates.

3.6. Changes in Ozone Loss Cycles and Ozone

The sign of the change in stratospheric ozone mixing ratios as the result of geoengineering is influenced by both chemical and dynamical changes and varies strongly with region (Figure 14, top panels) as also discussed in detail in Tilmes et al. (2009). Changes in the net chemical production (production minus loss) of ozone (Figure 14, bottom panels) depend mainly on two factors, the change in stratospheric aerosol burden and the amount of halogens and, therefore, the equivalent effective chlorine in the stratosphere, resulting in changes in SAD, temperature, and water vapor. The difference in changes between ozone mixing ratios (top panels) and net production rates (bottom panels) of Figure 14 can therefore be attributed to differences in advection of ozone.

The enhanced aerosol burden results in changes in the photochemical production of ozone and different ozone-destroying cycles. Changes of two heterogeneous reactions are most important:

$$N_2O_5 + H_2O \quad \rightarrow \quad 2HNO_3 \tag{1}$$

$$ClONO_2 + H_2O \quad \rightarrow \quad HOCl + HNO_3 \quad \text{for} \quad T < 200\,K \tag{2}$$

$$ClONO_2 + HCl \quad \rightarrow \quad Cl_2 + HNO_3 \quad \text{for} \quad T < 200\,K \tag{3}$$

Figure 13. As Figure 11 but for N_2O, CFC12, NO_y, and ClO_y.

The loss of reactive nitrogen (NO_x) via hydrolysis of dinitrogen pentoxide (N_2O_5; e.g., Fahey et al., 1993) decreases the rate of the catalytic NO_x ozone loss cycle and increases the rate of the ozone loss cycles involving reactive chlorine (ClO_x), bromine (BrO_x), and hydrogen (HO_x) families (equation (1)). This reaction is dominant in the tropical midstratosphere (Figure 15, middle column) and midlatitudes (not shown). A change in the SAD and NO_y would result in a change of the importance of this process, although this effect could saturate at very high aerosol loadings (e.g., Berthet et al., 2017). The larger increase in SAD at higher altitudes in the high-altitude injection case (Figure 5, second row) results in a larger decrease in odd nitrogen ozone loss rates, and a slightly stronger decrease in the total loss rates than in the low-altitude injection case (Figure 15, middle row and middle column, blue versus red lines).

The hydrolysis of chlorine nitrate ($ClONO_2$) results in the production of hypochlorous (HOCl), increased HO_x and ClO, and increased ozone loss via the catalytic ClO_x and HO_x cycles (equation (2)). Heterogeneous
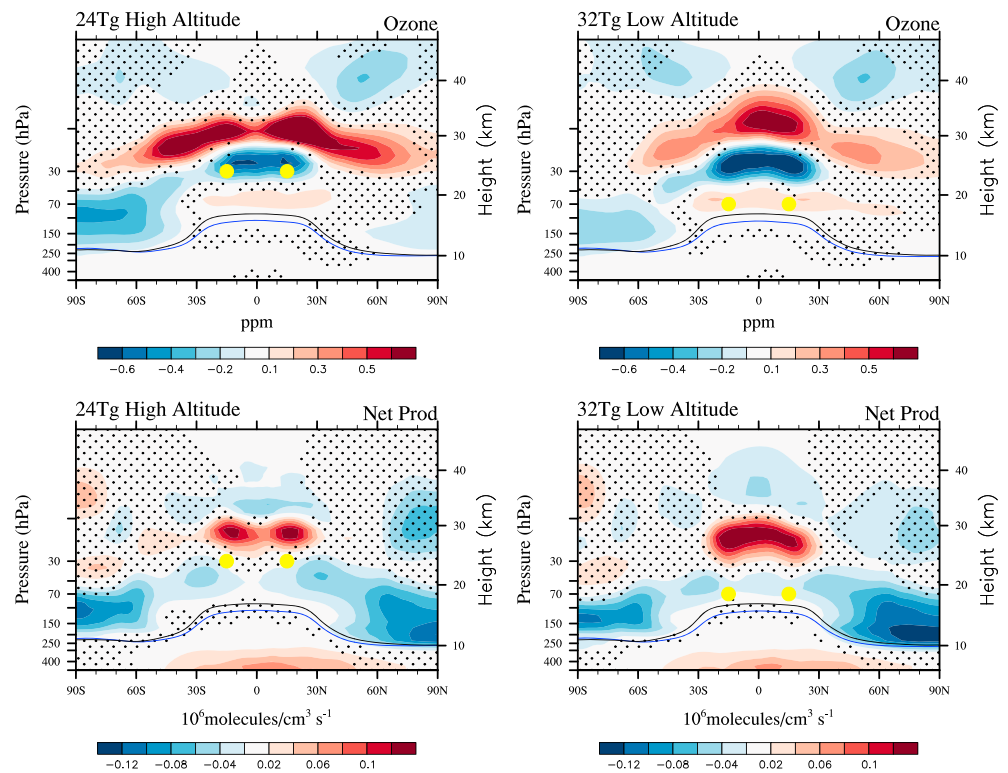
Figure 14. As Figure 5 but for ozone (top) and net chemical ozone production rates (bottom).

reactions of ClONO$_2$ with hydrogen chloride (HCl) result in additional reactive chlorine (equation (3)). The increase in SAD in addition to the occurrence of polar stratospheric clouds make this reaction especially important at low temperatures in the lower stratosphere in winter and spring polar regions (Figure 15, bottom row, right and left panels). Additional reactions, including the hydrolysis of BrONO$_2$, play important roles in warmer conditions (Tilmes et al., 2012), as recent observations after small volcanic eruptions have demonstrated (Berthet et al., 2017). The importance of these reactions declines with the projected decrease in stratospheric halogen concentration. The stronger increase in ClO$_x$ and BrO$_x$ rates over the SH polar regions for the high-altitude injection case is due to the enhanced SAD at altitudes above 100 hPa.

The increase of the cold point temperature and the resulting increase in stratospheric water vapor content leads to an additional increase in the HO$_x$ cycle-mediated ozone loss throughout the stratosphere, especially in spring and summer. The resulting changes in net chemical ozone production are most important in the lower and upper stratosphere, especially in the spring and summer in the NH. Changes in the odd hydrogen cycle are more important for the low-altitude injection case, since water vapor has increased by about 4 ppm for the low-altitude injection case, compared to about 2 ppm for the high-altitude injection case (Figure 8). Changes in the odd oxygen loss rates are impacted by changes in stratospheric temperatures. The stronger heating for the high-altitude injection case above 25 hPa results in increased odd oxygen rates compared to the low-altitude injection case. As shown by Tilmes et al. (2009), changes in the ozone profile as a result of geoengineering are a combination of chemical ozone loss, production, and advection. Changes in advection as described in section 3.4 have an important impact on ozone mixing ratios in both tropics and high latitudes. Despite similar or even stronger reductions in the net chemical production of high latitude lower stratospheric ozone in the low-altitude injection case, ozone mixing ratios do not significantly decrease, unlike in the high-altitude injection case, due to differences in horizontal and vertical advection (Figure 15, top panel). Therefore, column-integrated ozone concentrations, especially in the NH middle and high latitudes, are strongly impacted by both chemical and dynamical changes.
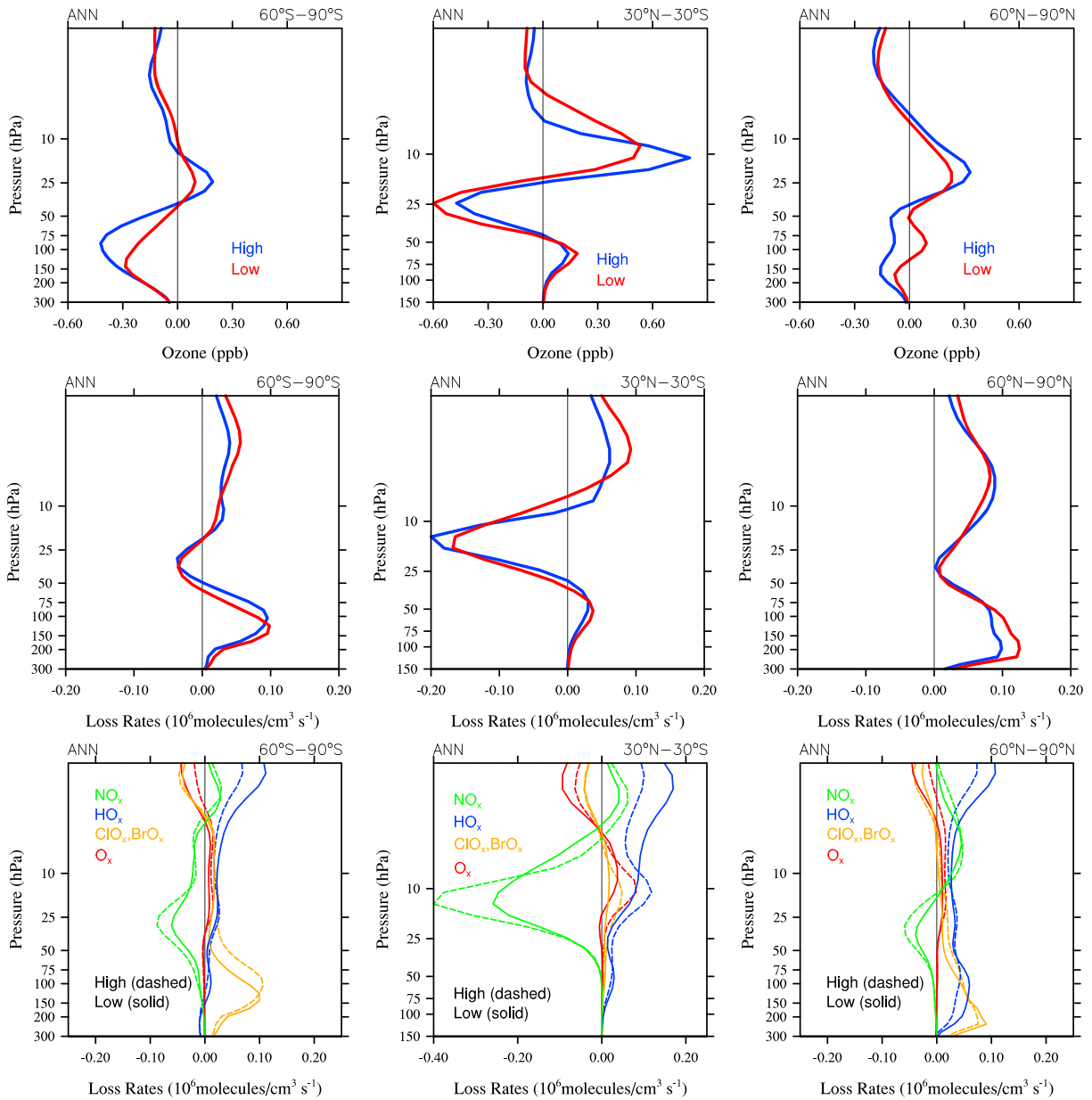
Figure 15. Difference between SO$_2$ injection simulations and the control simulation for annually averaged values between 30°N and 30°S and averaged for 2042 and 2049, for ozone mixing ratios (top row), total chemical loss rates (middle row), and ozone loss cycles (bottom row).

4. Summary and Conclusions

In this study, the impact of SO$_2$ injections on stratospheric chemistry and dynamics has been investigated using SO$_2$ injections at two different altitudes at about 1 and 5 km above the tropical tropopause, with equal and simultaneous injections at 15°N and 15°S. The two cases required different masses to be injected in order to achieve the same surface cooling. High-altitude injection at 25 km required 24 Tg SO$_2$/year. Low-altitude injection at about 20 km required 32 Tg SO$_2$/year and, therefore, 33% more SO$_2$ than the high injection case. Both cases resulted into a surface cooling of about 2°C in our model. Differences in the injection altitude (and amount) result in a significantly different response in the stratospheric dynamics including transport, temperature, and water vapor, as well as tracer distribution, including ozone, as the result of chemical and dynamical changes. The injections lead to an increase in temperature in the tropical stratosphere of up to 10 and 15°C, and increase in the tropical cold point temperature of about 5 to 7°C for the high and low injection cases, respectively, as the result of changes in radiative and dynamical heating caused by the increased aerosol mass

and corresponding changes in ozone (Richter et al., 2017). Consequently, water vapor mixing ratios increase by up to 4 ppm and therefore double in the low-altitude injection case, while they increase by up to 2 ppm for the high-altitude injection case.

Net chemical production rates of ozone respond primarily to the change in SAD, with secondary effects due to changes in chemical tracers and stratospheric water vapor. Additionally, differences in the aerosol distribution result in differences in stratospheric temperature and heating rates between the two injection experiments leading to changes in dynamics. While both SO_2 injection cases show an increase in the BDC strength and increased transport toward the NH, the low-altitude injection case results in increased tracer transport from the tropics to high latitudes in the lower stratosphere above about 75 hPa, beyond that of the high-altitude injection case. The stronger transport of higher ozone mixing ratios from the tropics to high latitudes in the low-altitude injection case counteracts the larger reductions in the net chemical ozone production in the polar lower stratosphere compared to the high-altitude injection case. This results in a stronger decrease in column ozone in the high-altitude injection case compared to 2042–2049 control conditions. The decrease in column ozone in polar regions mostly counteracts ozone recovery by the middle of the century and does not show significant reductions below values from observations and the model for the period 2004–2010. On the other hand, the larger tracer transport for the low injection case causes ozone to increase up to 8% in winter in middle and high latitudes as compared to the control conditions in 2042–2049. Despite the very large SO_2 injection rates, in both cases the QBO does not disappear as suggested by earlier studies. In fact, in the high-altitude injection simulation, the QBO is more similar to that in 2000–2010 than the QBO in the control simulation between 2040 and 2049 (not shown).

The zonally averaged seasonal changes in column ozone as the result of SO_2 injections agrees with earlier studies by Tilmes et al. (2009) and Pitari et al. (2014). However, here, we also find an increase in column ozone in winter middle and high northern latitudes as the result of stratospheric aerosol geoengineering. Compared to Tilmes et al. (2009), the decreases in SH polar ozone column of up to 40% in this study is much larger than about 15% in Tilmes et al. (2009), and reductions in column ozone during March over the NH polar region are stronger. Differences are likely a result of the larger injection amount in this study but also due to a much improved representation of dynamical processes, aerosol formation, and chemical response in the model. A potential change in the response of the high- and low-altitude injection cases with a smaller or larger injection amount has to be investigated in future studies.

This study was performed for equal and simultaneous injections at two latitudes and was not intended to strategically counteract climate change or to achieve specific climate goals, as demonstrated by Kravitz et al. (2017). We have used a fixed amount of SO_2 injection over 10 years for the period between 2040 and 2049 using the RCP8.5 climate scenario. Our results strongly depend on the specific amount of ozone depleting substances (ODS) present in the stratosphere as well as the burden of other tracers, including N_2O and methane. While the importance of ClO_x and BrO_x cycles is expected to decrease with time, dynamical differences between high and low injection cases are not expected to change. We have chosen very large injection amounts that would produce a cooling of $\approx$2°C from the RCP8.5 scenario in 2040–2049 toward temperatures closer to the year 2000. A climate scenario with lower greenhouse gas concentrations would require less SO_2 mass injections to reach similar surface temperature conditions, so the relative change in column ozone would be smaller if applying geoengineering. However, it would also result in different baseline conditions compared to present day, depending on details of the emission scenario. Further work is required to understand the impact of changing ODS, greenhouse gases, and changing aerosols loading in the stratosphere. Specifics of the aerosol distribution and size, and the dynamical response of geoengineering, is also strongly model dependent (Visioni, Pitari, & Aquila, 2017). For example, differences in the response to cirrus clouds, changes in water vapor, and methane lifetime, between different models, can change the surface cooling efficiency of geoengineering and therefore would require different injection amounts that could impact stratospheric dynamics and chemistry.

Stratospheric dynamic and chemical responses to different injection altitudes need to be considered in addition to considerations of efficiency in surface temperature reduction per injection amount with altitude, when deciding what injection altitudes may be chosen for developing geoengineering strategies. In regard to column ozone changes, resulting impacts need to be further investigated, including changes in surface UV,

tropospheric chemistry and air quality, and impacts on the biosphere. Fully coupled models that interactively consider chemistry, radiation and dynamics, and UV adjustments are required to identify the full range of impacts of geoengineering with regard to stratospheric changes.

References

Berthet, G., Jegou, F., Catoire, V., Krysztofiak, G., Renard, J.-B., Bourassa, A. E., et al. (2017). Impact of a moderate volcanic eruption on chemistry in the lower stratosphere: Balloon-borne observations and model calculations. *Atmospheric Chemistry and Physics*, *17*, 2229–2253. https://doi.org/10.5194/acp-17-2229-2017

Birner, T., & Bönisch, H. (2011). Residual circulation trajectories and transit times into the extratropical lowermost stratosphere. *Atmospheric Chemistry and Physics*, *11*, 817–827. https://doi.org/10.5194/acp-11-817-2011

Butler, A. H., Daniel, J. S., Portmann, R. W., Ravishankara, A. R., Young, P. J., Fahey, D. W., & Rosenlof, K. H. (2016). Diverse policy implications for future ozone and surface UV in a changing climate. *Environmental Research Letters*, *11*, 064017. https://doi.org/10.1088/1748-9326/11/6/064017

Computational and Information Systems Laboratory (2012). Yellowstone: IBM iDataPlex System (NCAR Strategic Capability Projects).

Crutzen, P. J. (2006). Albedo enhancements by stratospheric sulfur injections: A contribution to resolve a policy dilemma? An Editorial Essay. *Climate Change*, *77*, 211–219.

English, J. M., Toon, O. B., & Mills, M. J. (2012). Microphysical simulations of sulfur burdens from stratospheric sulfur geoengineering. *Atmospheric Chemistry and Physics*, *12*(10), 4775–4793. https://doi.org/10.5194/acp-12-4775-2012

Fahey, D., Kawa, S., Woodbridge, E., Tin, P., Wilson, J., Jonsson, H., et al. (1993). In situ measurements constraining the role of sulphate aerosols in mid-latitude ozone depletion. *Nature*, *363*, 509–514.

Heckendorn, P., Weisenstein, D., Fueglistaler, S., Luo, B. P., Rozanov, E., Schraner, M., et al. (2009). The impact of geoengineering aerosols on stratospheric temperature and ozone. *Environmental Research Letters*, *4*, 045108. https://doi.org/10.1088/1748-9326/4/4/045108

Hegglin, M. I., & Shepherd, T. G. (2007). O_3-N_2O correlations from the {Atmospheric Chemistry Experiment}: {Revisiting} a diagnostic of transport and chemistry in the stratosphere. *Journal of Geophysical Research*, *112*, D19301. https://doi.org/10.1029/2006JD008281

Ivy, D. J., Solomon, S., Kinnison, D., Mills, M. J., Schmidt, A., & Neely, R. R. (2017). The influence of the Calbuco eruption on the 2015 Antarctic ozone hole in a fully coupled chemistry-climate model. *Geophysical Research Letters*, *44*, 2556–2561. https://doi.org/10.1002/2016GL071925

Kleinschmitt, C., Boucher, O., & Platt, U. (2017). Sensitivity of the radiative forcing by stratospheric sulfur geoengineering to the amount and strategy of the SO_2 injection studied with the LMDZ-S3A model. *Atmospheric Chemistry and Physics Discussions*, 1–34. https://doi.org/10.5194/acp-2017-722

Kravitz, B., MacMartin, D. G., Mills, M. J., Richter, J. H., Tilmes, S., Lamarque, J.-F., et al. (2017). First simulations of designing stratospheric sulfate aerosol geoengineering to meet multiple simultaneous climate objectives. *Journal of Geophysical Research: Atmospheres*, *122*, 12,616–12,634. https://doi.org/10.1002/2017JD026874

MacMartin, D. G., Kravitz, B., Tilmes, S., Richter, J. H., Mills, M. J., Lamarque, J.-F., et al. (2017). The climate response to stratospheric aerosol geoengineering can be tailored using multiple injection locations. *Journal of Geophysical Research: Atmospheres*, *122*, 12,574–12,590. https://doi.org/10.1002/2017JD026868

Meinshausen, M., Smith, S. J., Calvin, K., Daniel, J. S., Kainuma, M. L. T., Lamarque, J.-F., et al. (2011). The RCP greenhouse gas concentrations and their extensions from 1765 to 2300. *Climatic Change*, *109*(1-2), 213–241. https://doi.org/10.1007/s10584-011-0156-z

Mills, M. J., Richter, J. H., Tilmes, S., Kravitz, B., MacMartin, D. G., Glanville, A. A., et al. (2017). Radiative and chemical response to interactive stratospheric sulfate aerosols in fully coupled CESM1(WACCM). *Journal of Geophysical Research: Atmospheres*, *122*, 13,061–13,078. https://doi.org/10.1002/2017JD027006

Morgenstern, O., Akiyoshi, H., Yamashita, Y., Kinnison, E., Garcia, R. R., Plummer, D. A., et al. (2017). Ozone sensitivity to varying greenhouse gases and ozone-depleting substances in CCMI simulations, (July) (pp. 1–32).

Newman, P. A., Nash, E. R., Kawa, S. R., Montzka, S. A., & Schauffler, S. M. (2006). When will the {A}ntarctic ozone hole recover? *Geophysical Research Letters*, *33*, L12814. https://doi.org/10.1029/2005GL025232

Niemeier, U., & Schmidt, H. (2017). Changing transport processes in the stratosphere by radiative heating of sulfate aerosols. *Atmospheric Chemistry and Physics Discussions*, *17*, 1–24. https://doi.org/10.5194/acp-2017-470

Niemeier, U., Schmidt, H., & Timmreck, C. (2011). The dependency of geoengineered sulfate aerosol on the emission strategy. *Atmospheric Science Letters*, *12*(2), 189–194. https://doi.org/10.1002/asl.304

Pierce, J. R., Weisenstein, D. K., Heckendorn, P., Peter, T., & Keith, D. W. (2010). Efficient formation of stratospheric aerosol for climate engineering by emission of condensible vapor from aircraft. *Geophysical Research Letters*, *37*, L18805. https://doi.org/10.1029/2010GL043975

Pitari, G., Aquila, V., Kravitz, B., Robock, A., Watanabe, S., Cionni, I., et al. (2014). Stratospheric ozone response to sulfate geoengineering: Results from the Geoengineering Model Intercomparison Project (GeoMIP). *Journal of Geophysical Research: Atmospheres*, *119*, 2629–2653. https://doi.org/10.1002/2013JD020566

Portmann, R. W., Solomon, S., Garcia, R. R., Thomason, L. W., Poole, L. R., & McCormick, M. P. (1996). Role of aerosol variations in anthropogenic ozone depletion in the polar regions. *Journal of Geophysical Research*, *101*(22), 22,991–23,006.

Richter, J. H., Tilmes, S., Mills, M. J., Tribbia, J. J., Kravitz, B., MacMartin, D. G., et al. (2017). Stratospheric dynamical response to SO_2 injections. *Journal of Geophysical Research: Atmospheres*, *122*, 12,557–12,573. https://doi.org/10.1002/2017JD026912

Solomon, S., Ivy, D. J., Kinnison, D., Mills, M. J., Neely, R. R., & Schmidt, A. (2016). Emergence of healing in the Antarctic ozone layer. *Science*, *353*, 269–274. https://doi.org/10.1126/science.aae0061

Tilmes, S., Garcia, R. R., Kinnison, D. E., Gettelman, A., & Rasch, P. J. (2009). Impact of geoengineered aerosols on the troposphere and stratosphere. *Journal of Geophysical Research*, *114*, D12305. https://doi.org/10.1029/2008JD011420

Tilmes, S., Lamarque, J.-F., Emmons, L. K., Conley, A., Schultz, M. G., Saunois, M., et al. (2012). Technical note: Ozonesonde climatology between 1995 and 2011: Description, evaluation and applications. *Atmospheric Chemistry and Physics*, *12*(16), 7475–7497. https://doi.org/10.5194/acp-12-7475-2012

Tilmes, S., Müller, R., Salawitch, R. J., Schmidt, U., Webster, C. R., Oelhaf, H., et al. (2008). Chemical ozone loss in the Arctic winter 1991–1992. *Atmospheric Chemistry and Physics*, *8*, 1897–1910.

Tilmes, S., Richter, J. H., Mills, M. J., Kravitz, B., MacMartin, D. G., Vitt, F., et al. (2017). Sensitivity of aerosol distribution and climate response to stratospheric SO_2 injection locations. *Journal of Geophysical Research: Atmospheres*, *122*, 12,591–12,615. https://doi.org/10.1002/2017JD026888

Visioni, D., Pitari, G., Aquila, V., Tilmes, S., Cionni, I., Di Genova, G., & Mancini, E. (2017). Sulfate geoengineering impact on methane transport and lifetime: Results from the Geoengineering Model Intercomparison Project (GeoMIP). *Atmospheric Chemistry and Physics*, *17*, 11,209–11,226. https://doi.org/10.5194/acp-17-11209-2017

Visioni, D., Pitari, G., & Aquila, V. (2017). Sulfate geoengineering: A review of the factors controlling the needed injection of sulfur dioxide. *Atmospheric Chemistry and Physics*, *17*, 3879–3889. https://doi.org/10.5194/acp-17-3879-2017

World Meteorological Organization (2010). Scientific assessment of ozone depletion.

World Meteorological Organization (2014). Scientific assessment of ozone depletion: 2014, Global Ozone Research and Monitoring Project-Report No.\ 51, Geneva, Switzerland.

World Meteorological Organization (1957). Meteorology — A three-dimensional science (pp. 134–138). WMO Bull 6.

Xia, L., Nowack, P. J., Tilmes, S., & Robock, A. (2017). Impacts of stratospheric sulfate geoengineering on tropospheric ozone. *Atmospheric Chemistry and Physics*, *17*, 11,913–11,928. https://doi.org/10.5194/acp-17-11913-2017

Ziemke, J. R., Chandra, S., Labow, G. J., Bhartia, P. K., Froidevaux, L., & Witte, J. C. (2011). A global climatology of tropospheric and stratospheric ozone derived from Aura OMI and MLS measurements. *Atmospheric Chemistry and Physics*, *11*(17), 9237–9251. https://doi.org/10.5194/acp-11-9237-2011